NASA/TM-20250001636



Large Area SiC LET Detectors for Space Science Applications

John D. Wrbanek and Susan Y. Wrbanek Glenn Research Center, Cleveland, Ohio

José M. Gonzalez and Beth A. Osborn HX5 Sierra, Inc., Fremont, Ohio

NASA STI Program Report Series

Since its founding, NASA has been dedicated to the advancement of aeronautics and space science. The NASA scientific and technical information (STI) program plays a key part in helping NASA maintain this important role.

The NASA STI program operates under the auspices of the Agency Chief Information Officer. It collects, organizes, provides for archiving, and disseminates NASA's STI. The NASA STI program provides access to the NTRS Registered and its public interface, the NASA Technical Reports Server, thus providing one of the largest collections of aeronautical and space science STI in the world. Results are published in both non-NASA channels and by NASA in the NASA STI Report Series, which includes the following report types:

TECHNICAL PUBLICATION.

Reports of completed research or a major significant phase of research that present the results of NASA programs and include extensive data or theoretical analysis. Includes compilations of significant scientific and technical data and information deemed to be of continuing reference value. NASA counterpart of peer-reviewed formal professional papers but has less stringent limitations on manuscript length and extent of graphic presentations.

TECHNICAL MEMORANDUM.

Scientific and technical findings that are preliminary or of specialized interest, e.g., quick release reports, working papers, and bibliographies that contain minimal annotation. Does not contain extensive analysis.

CONTRACTOR REPORT. Scientific and technical findings by NASA-sponsored contractors and grantees.

CONFERENCE PUBLICATION. Collected papers from scientific and technical conferences, symposia, seminars, or other meetings sponsored or cosponsored by NASA.

SPECIAL PUBLICATION.

Scientific, technical, or historical information from NASA programs, projects, and missions, often concerned with subjects having substantial public interest.

TECHNICAL TRANSLATION.

English-language translations of foreign scientific and technical material pertinent to NASA's mission.

Specialized services also include organizing and publishing research results, distributing specialized research announcements and feeds, providing information desk and personal search support, and enabling data exchange services.

For more information about the NASA STI program, see the following:

 Access the NASA STI program home page at http://www.sti.nasa.gov

NASA/TM-20250001636



Large Area SiC LET Detectors for Space Science Applications

John D. Wrbanek and Susan Y. Wrbanek Glenn Research Center, Cleveland, Ohio

José M. Gonzalez and Beth A. Osborn HX5 Sierra, Inc., Fremont, Ohio

National Aeronautics and Space Administration

Glenn Research Center Cleveland, Ohio 44135

Acknowledgments

This work was performed at NASA Glenn Research Center and sponsored by the NASA Glenn Innovation and Integration Office through the Independent Research and Development (IRAD) Program. The authors are appreciative of Elizabeth McQuaid, formerly of NASA Glenn, for assembling the detectors at the beginning of this effort before her retirement. Also, the authors are grateful for the Auger electron spectroscopy depth analysis of the metallization performed by Dr. Sean McDarby of the Universities Space Research Association, supporting the Smart Sensing and Electronics Systems Branch at NASA Glenn. The authors would like to thank Dr. Srihari Rajgopal and Diana Centeno-Gomez (chief) of the Smart Sensing and Electronics Systems Branch for their review and comments on this work.

This report is a formal draft or working paper, intended to solicit comments and ideas from a technical peer group.

This report contains preliminary findings, subject to revision as analysis proceeds.

Trade names and trademarks are used in this report for identification only. Their usage does not constitute an official endorsement, either expressed or implied, by the National Aeronautics and Space Administration.

Level of Review: This material has been technically reviewed by technical management.

This report is available in electronic form at https://www.sti.nasa.gov/ and https://ntrs.nasa.gov/

Large Area SiC LET Detectors for Space Science Applications

John D. Wrbanek and Susan Y. Wrbanek National Aeronautics and Space Administration Glenn Research Center Cleveland, Ohio 44135

José M. Gonzalez and Beth A. Osborn HX5 Sierra, Inc. Fremont, Ohio 43420

Summary

The wide band gap and high displacement energy of silicon carbide (SiC) give it thermal stability and radiation hardness properties to make it attractive as Linear Energy Transfer (LET) radiation detectors for harsh environments. Large area detectors of 2 cm² and larger are required for space science applications, introducing challenges of noise and energy resolution due to the size. This study improves on the previous work in this area, demonstrating alpha particle energy resolution of under 0.1 dE/E, nearing the limit of the diffusion of the source particles in air, with leakage current consistently under 1 nA. Polarization effects are observed but can be mitigated with pulsed biasing. The importance of silicon on the metallization interfaces is noted and suggests a path towards more improvements in detector design for future work.

Introduction

The manner and extent of the impact of high energy ions in the form of solar energetic particles (SEPs) and galactic cosmic rays (GCRs) on planetary magnetosphere, atmosphere, and surface (space weathering) processes are not systematically known. Heavy ions in GCR are suspected to have a role in processes as diverse as space weathering, cloud formation, and magnetospheric shaping (Refs. 1 to 3). Transport effects related to charged particle anisotropies are particularly important in the acceleration of SEPs from coronal and interplanetary disturbances (Ref. 4). On bodies lacking strong magnetospheres and true atmospheres, such as the Moon, energetic ions interact directly with the surface, and play an important role in space weathering, redistribution of volatiles, and polymerization of organic materials, through radiation chemistry.

In order to provide a complete understanding of how energetic processes internal and external to the solar system shape magnetospheres, atmospheres, and surfaces, in situ particle observations should include measurements of SEPs and GCR, along with solar wind and plasma. The ability to monitor these fluxes in multiple directions simultaneously will enable the ability to distinguish SEP and GCRs and their respective spectra. Missions to achieve these measurements would include flexible path orbiters, probes, landers or rovers beyond low Earth orbit (LEO).

To that end, the "Space Weather Science and Observational Gap Analysis for the National Aeronautics and Space Administration" (2021) (Ref. 5) specifically calls out the need for measurements of SEP occurrence and properties as the top ranked (#1) space weather observation and research gap. Measurement of fine-scale structure of solar wind transients and spatiotemporal evolution and turbulence measurements is the third-ranked (#3). The report calls out multipoint (grid) in-situ particle and fields measurement as a high priority for improving critical gaps (priority I3), and measurements of radially distributed particles and fields a high priority for advancing critical gaps (priority A2).

Small satellites with mass less than 100 kg (such as CubeSats) are seen to be low-cost platforms ideal for conducting this range of observations either solo or in multiple locations as a swarm. However, current detector technology limits the measurement capability by restrictions of size, power, and thermal stability of the small satellite platform. Current state-of-the-art (SOA) in solid-state space radiation detectors are derived from Earth-based applications, transitioning existing technology from nuclear research to space-based science platforms. An increasing demand for low size, power, and cost restrictions of instruments that need to fit on small satellite platforms forces a reconsideration of this approach.

To meet the challenges of low-power, low-noise, multidirectional robust detectors for a wide range of mass and energies, new ion detectors based on wide band gap (WBG) semiconductors are under development at NASA's Glenn Research Center (GRC) for integration into small satellite platforms (Ref. 6). As these WBG semiconductor detector technologies advance, more comprehensive (composition, velocity, and direction) in-situ measurements of heavy ions and space plasmas in deep space environments will be made possible on small satellite platforms.

The wide band gap and high displacement energy of silicon carbide (SiC) make it attractive as Linear Energy Transfer (LET) detectors. Sensors and electronic devices made from SiC have much better resistance to radiation damage from energetic charged particles that can form defects in the semiconductor than silicon devices (Ref. 7). The wide band gap nature of SiC also allows measurements made by the detectors to be unaffected by thermal drift due to sun/shade transitions unlike silicon devices.

Micro-electro-mechanical-system (MEMS) based devices fabricated from silicon carbide (SiC) for the purpose of conducting low-noise neutron and alpha particle spectrometry have been reported in the context of reactor core monitoring (Ref. 8). A low power, low mass space radiation detector prototype system using a SiC Schottky power diode was developed at GRC for dosimetry use during future lunar missions (Ref. 9).

Another issue for science instrument designs is sensitivity in the space environment. The sensitivity of a particle detector is directly proportional to its geometric factor, in units of steradians cm². For compact stacked detectors, used in a charged particle telescope (CPT) configuration, the geometric factor is the product of the areas of the entrance window and the exit window (or detector) divided by the square of the distance between the two (Ref. 10). Thus, the greater the area of the detector, the greater the geometric factor and higher the sensitivity. Large area detectors are required for space science applications, with the larger size introducing challenges to noise and energy resolution.

As part of the formulation of a deep-space interplanetary science CubeSat concept, large area (2 cm²) SiC radiation detectors based on High Purity Semi-Insulating (HPSI) SiC were fabricated and demonstrated as proof-of-concept devices (Ref. 11). In that work, the devices were shown to have a leakage current of 4.5 nA at 100 V bias, similar to Si detectors of half the area, and sensitive to 26.3 keV gamma rays emitted from a Pu-239 alpha source with a dE/E resolution of 0.2. Minimum LET measured by the detectors was 28 eV/g/m². Based on the results of that work, further development is undertaken to improve the large area SiC radiation detectors for future space science and space weather monitoring applications.

Detector Design and Fabrication

The semiconductor detector design is a PN diode with a depleted region between the two p and n regions (Refs. 12 and 13). This region is formed by biasing the voltage to sweep the free charges in these regions to the contacts. It is in this depleted region that electron-hole pairs are formed by ionizing radiation. The charges drift to the contacts in the electric field and a current spike proportional to the ionization energy deposited in the detector is recorded by the signal conditioning electronics.

To increase the sensitivity of particles passing through the detector, the depleted region should be large and with minimal dead space at the contact regions. The use of vanadium-free high purity semi-insulating (HPSI) SiC is attractive since the wafer is depleted as-is, making the entire thickness of the wafer the active region (350 to 500 μ m), ideal for detecting high energy ions.

For the contacts, platinum is chosen as the anode for its high work function up to 5.9 eV (Refs. 14 and 15), and nickel is chosen as the cathode due to reactivity with silicon (Ref. 16). Gold overcoat on nickel is required for electrical bonding (Refs. 17 to 19). For high temperature conditions where platinum reacting with silicon is an issue, iridium with a work function up to 5.7 eV can be used as an alternative.

The detectors are fabricated at the NASA Glenn Research Center Microsystem Fabrication Laboratory from scratch and assembled on-site. To fabricate the detecting elements, a HPSI 4H SiC wafer is cleaned using a buffered HF oxide etch (BOE) and piranha etch with a H₂SO₄/H₂O₂ solution (P-clean). After the initial cleaning, the wafer is put through a dry oxidation at 1150 °C followed by another round of BOE and P-Clean.

The cathode contact is formed on the back side of the wafer with a sputtered layers of 100 nm nickel with a 1 nm titanium bond coat and an overcoat of 1000 nm gold, coating the entire wafer and is not patterned. As is typical for Ni-based contacts (Refs. 20 and 21), the wafer is annealed at 1000 °C for 5 min in a pure nitrogen atmosphere.

The anode contact is formed by coating the front side of the wafer with sputtered 100 nm platinum with a 1 nm titanium bond coat, followed with a 348 °C bakeout before and after deposition to minimize stress of the films. The anode pattern is formed with photolithography and dry etched using a 6 mTorr argon plasma at 100 W(RF) for 1 h. The wafer is then diced and rinsed to ready the detectors for packaging.

A schematic of the detector layers is show in Figure 1(a) with a photo of four produced detectors shown in Figure 1(b). A SiC wafer typically has silicon atoms on the surface of one side (the Si-face), and carbon atoms on the surface of the other (the C-face). To investigate if there is a performance difference between using the either the Si-face or C-face as the front side for the anode, two different types of detectors were fabricated. For the first type, the Si-face of the SiC wafer was patterned as the anode and the C-face of the wafer was coated as the cathode. For the second type of detector the C-face of the SiC wafer was patterned as the anode and the Si face was coated as the cathode.

The detector case is designed to house the sensor in a single LET detector configuration, or alternatively multiple cases can be stacked as a telescope configuration. The LET configuration is shown firstly as a 3D modeled schematic (Figure 2(a)) and secondly in the as-built assembly (Figure 2(b)). The case was milled from aluminum 6061 alloy by an outside vendor. The baseline detector has an outside diameter of 3.8 cm. A 2 mm notch and lip insure alignment between stacked detectors. The height of the

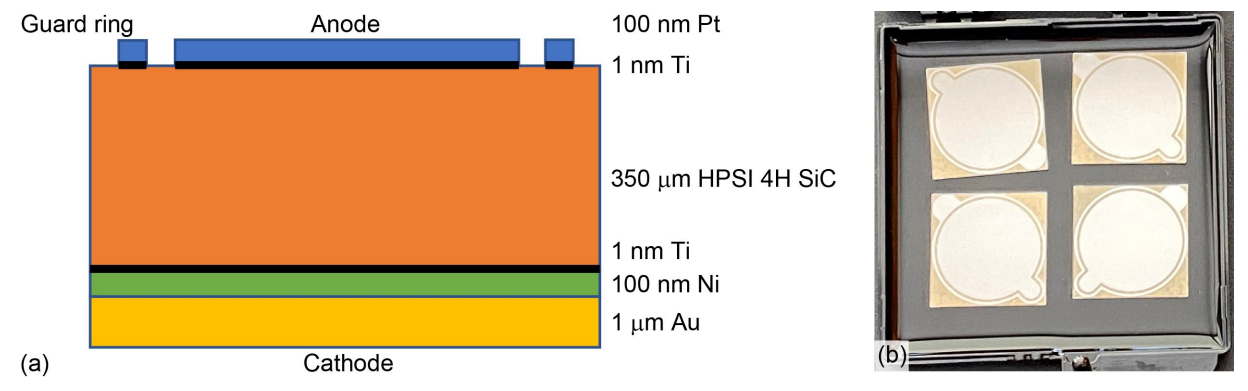


Figure 1.—SiC detectors. (a) Diagram of detector layers. (b) Photograph of four completed detectors.

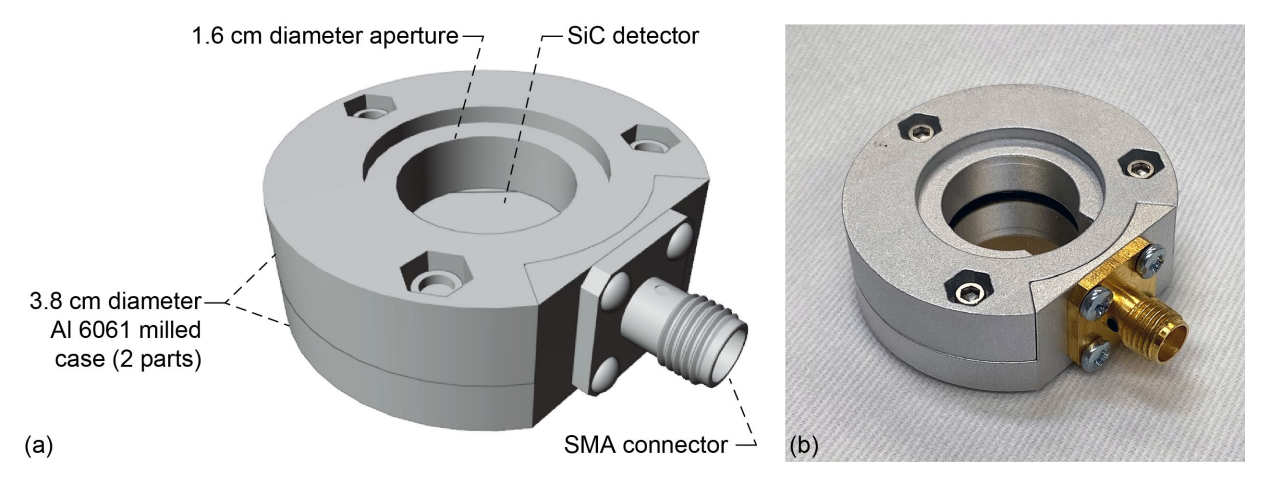


Figure 2.—Detector assembly. (a) Schematic. (b) Photograph of completed assembly.

sensor-containing portion of the frame is 1.27 cm, plus an additional 0.2 cm for the lip, resulting in an overall height of 1.47 cm. The baseline unit has a 1.6 cm diameter aperture accommodating the 2 cm² anode. The detector is held in place by an insulating fiberglass washer and lies 9.4 mm from the top aperture. The case has a SMA female connector that allows bias voltages up to 1000 V to be applied. The mass of the detector in the case is about 31 g.

Four detectors from each batch were assembled and tested, labeled as detectors A-D for the batch with the Si-face patterned as the anode, and E-H for the batch with the C-face patterned as the anode.

Detector Characterization

IV Curves

Current-voltage (IV) curves were taken for all detectors with the data shown in Figure 3(a) and (b). Voltage was supplied from -100 to +100 V and the current was measured using a four-wire method. The resolution of the current measurements was 0.1 nA.

The IV characteristics verified that the detectors are diodes to varying degrees. Under reverse bias, all detectors had dark currents less than -1 nA at -100 V, with an average of -0.26 nA. These values are about 1/6 smaller than the leakage expected from Si devices of half the area at the same bias (Ref. 6).

The capacitances of the devices were measured at 100 kHz, 1 V peak to peak using an LCR meter. The capacitance data with the DC leakage current at ± 100 V is shown in Table I. The expected capacitance assuming a dielectric constant of 9.66 (Ref. 22) with a separation of the electrodes of 350 μ m is 48.9 pF. The capacitance measured in detectors A-D were 17 percent higher and in detectors E, F, and H were 11 percent higher than this value, with detector G having less than half that capacitance. The implication with the measurements is that the effective region between the electrodes is reduced from the 350 μ m thickness, with detectors A-D more than detectors E, F, and H. Detector G's lower relative capacitance cannot be explained by that and remains an anomalous reading.

The detectors were then characterized for sensitivity to charged particles under reverse bias.

Spectroscopy Response

The detector sensitivity to alpha particles is measured by exposing the detector to an alpha source (either Am-241 or Pu-239) and monitoring the output on a multichannel analyzer (MCA). The detector under test is connected to a charge pre-amplifier which supplies high voltage bias to the detector. The

output of the pre-amplifier is input to a spectroscopy amplifier which performs pulse shaping, baseline recovery, and pile-up rejection on the signal. Shaping time of the pulse is set to 3 μ s to minimize noise. A schematic of the testing setup is shown in Figure 4.

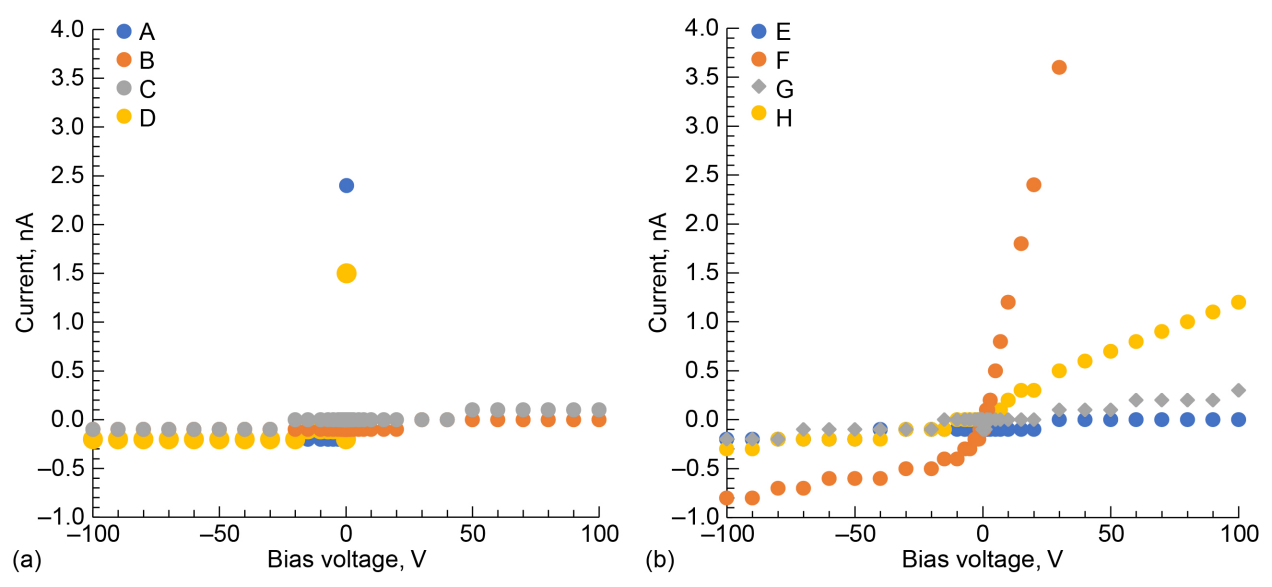


Figure 3.—IV curves. (a) Si-face anode detectors A-D. (b) C-face anode detectors E-H.

TABLE I.—ELECTRICAL CHARACTERISTICS OF THE SiC DETECTORS

Detector	Capacitance/dissipation at 0 V bias (±0.5%)	Leakage at –100 V bias (±0.1 nA)	Leakage at +100 V bias (±0.1 nA)
A	58.8 pF / -0.057	-0.2 nA	+301 μΑ (±0.1 μΑ)
В	58.8 pF / -0.058	-0.1 nA	+0.0 nA
С	58.6 pF / +0.047	−0.1 nA	+0.1 nA
D	58.8 pF / -0.056	−0.2 nA	+23.8 μΑ (±0.1 μΑ)
Е	55.0 pF / -0.055	−0.2 nA	+0.0 nA
F	54.9 pF / -0.055	−0.8 nA	+8.9 nA
G	22.6 pF / -0.036	−0.2 nA	+0.3 nA
Н	55.0 pF / -0.055	−0.3 nA	+1.2 nA

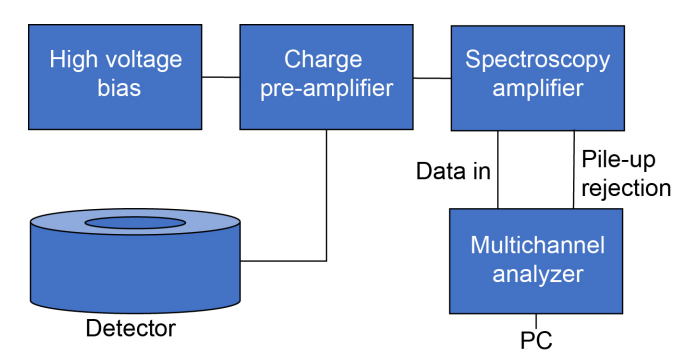


Figure 4.—Spectroscopy schematic with MCA data collection.

The output of the amplifier is input to an MCA along with the pile-up rejection signal for display on a PC. MCA integration time was set to 100 s in the initial studies. Initial characterization was performed on Detector F with the Am-241 alpha source under reverse bias at various voltages held for at least 12 min before recording a pulse-height spectrum. The peak bin and noise floor of the collected spectra with corresponding signal-to-noise, full width half-maximum (FWHM), and fractional energy resolution (dE/E) is shown in Table II. The collected spectra are shown in Figure 5. Based on these results, a bias of –200 V appears to be the optimal setting.

TABLE II.—DETECTOR F CHARACTERISTICS AT VARIOUS BIAS VOLTAGES

Bias (V)	Background bin (noise floor) (±1%)	Am-241 alpha peak bin (±1%)	Signal-to-noise ratio (±2%)	FWHM bins (±2%)	dE/E (±0.02)
-100	211	427	2.02	217	0.216
-200	216	1760	8.15	588	0.142
-300	381	1914	5.02	831	0.184
-400	566	2332	4.12	1048	0.191
-500	762	2775	3.64	1369	0.210
-600	937	3052	3.26	1604	0.223
-700	1089	3222	2.96	1612	0.213
-800	1199	3365	2.81	1893	0.239
-900	1309	3408	2.60	1884	0.235
-1000	1539	3502	2.28	2081	0.252

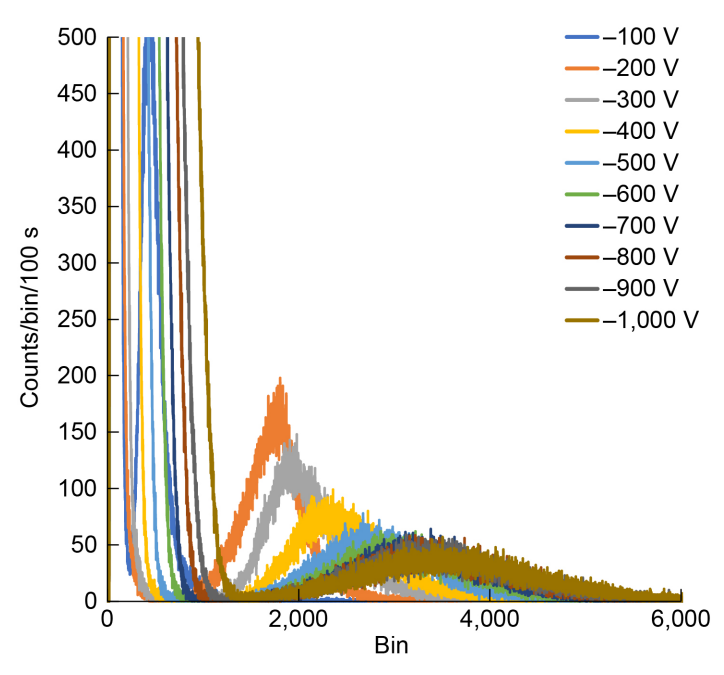


Figure 5.—Comparison of sensitivity spectrum of detector F at various bias voltages.

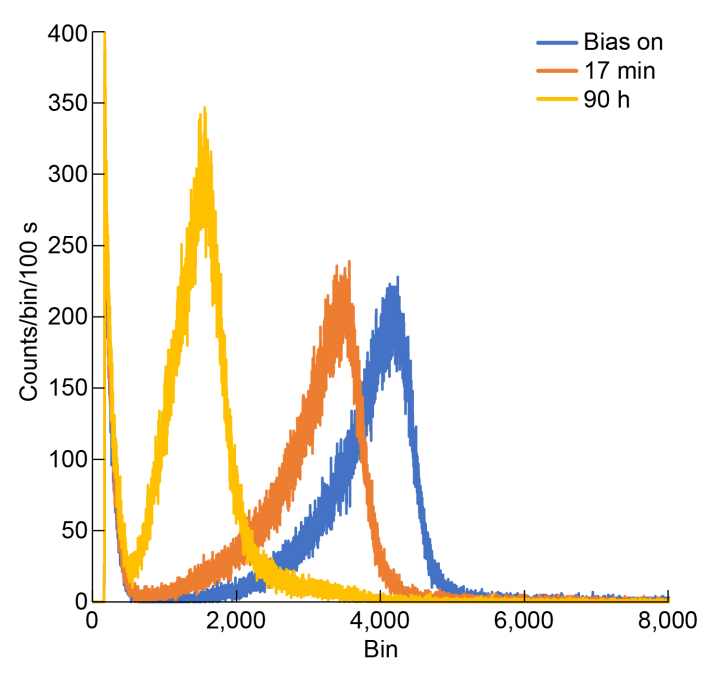


Figure 6.—Deposited energy spectra for detector F at –200 V bias exposed to Pu-239 alpha particles for 100 s at various elapsed times from turning on bias voltage.

Polarization Effects

One characteristic that was observed is a reduction in sensitivity of the detectors with time. This reduction is believed to be caused by a polarization effect of the semiconductor reported by other researchers (Ref. 23) wherein defects in the semiconductor trap charges due to the biasing of the detector. These traps reduce the depleted region where electron-hole pairs can form when irradiated, and thus lower the efficiency of the detector. This effect is dependent on the purity of the semiconductor, the number of defects, and detector capacitance. This effect is similar, but less than polarization effects that have been reported when diamond has been used as the semiconductor (Refs. 24 and 25).

The polarization effect we observed occurs upon biasing the detector, not upon exposure to an active radiation source. Polarization effects were observed for all of the detectors and for all bias voltages from -100 to -1000 V. An example is shown for Detector F biased at -200 V reacting to a Pu-239 alpha source. The signal shift with time is shown in Figure 6. After 90 h (5400 min) of biasing, the peak signal level was at 35 percent of that of the first minute.

The energy peak drop with time was examined in detail for Detector F at -200 V bias using a Pu-239 alpha source. The data sets are shown in Figure 7, and a curve was fitted to the data. The fitted curve follows Equation (1) with $R^2 = 0.9969$.

Peak Bin =
$$4226.2 \cdot (T)^{-0.18} + 610$$
 (1)

The elapsed time (T) in Figure 7 and Equation (1) is the time in minutes the bias supply is on. The source is not on the detector the entire time, but secured away from the detectors when the lab is not occupied. The fitted curve of Equation (1) to the decay of the energy peak appears to follow a $T^{-0.18}$ relationship, suggesting less than 0.1 percent per minute drift after 138 min of biasing. The fit also suggests at $T \to \infty$, the peak stabilizes to 14 percent of the value in the first minute.

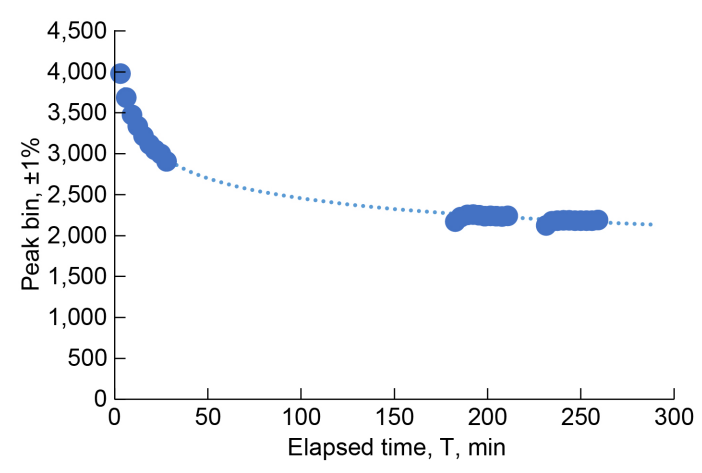


Figure 7.—Peak bin on MCA for detector F exposed to Pu-239 alpha source plotted against time detector is biased at –200 V with a fitted curve.

A slight decrease of the peak bin at the beginning of the latter two runs was observed when the Pu-239 alpha source was placed on the detector. This drop is approximately 64 and 87 bins or 3 to 4 percent of the maximum peak of the second run, and persists for about 10 min, suggesting a second, shorter-lived charge trapping effect due to the alpha particles.

Pulsed Bias Operation

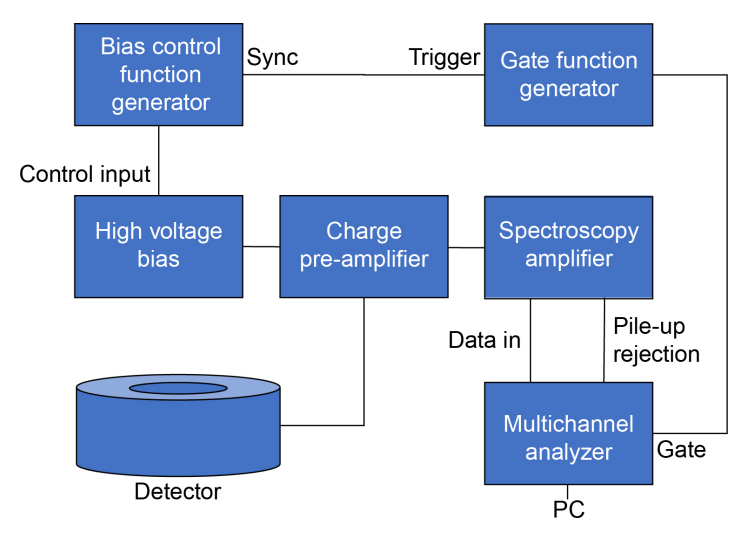
As noted above, significant polarization effects have been reported during operation (Ref. 23). Detectors based on diamond epilayers are also known to have significant polarization effects in operation reported to be mitigated by turning off the bias voltage for a time (Ref. 24) or reversing the polarity of the bias voltage to drive the collected charges away from their trapping sites (Ref. 25). For our thick, large area LET detectors using HPSI 4H SiC where high voltage biasing is needed, switching bias polarity quickly is not practical.

The method we implemented cycles the bias power supply remotely using a square wave from a controlling function generator. The square wave first biases the detector, then turns the detector off. Our detectors with the charged preamplifiers and biasing system used were found take about 80 s to achieve full biasing and another 80 s after turned off to become fully unbiased.

To prevent data collection during the ramp up and ramp down of the bias, a gate is generated using a second function generator in sync with the power supply controlling function generator as outlined in Figure 8. The result is that data collection is during a portion of the control cycle, enabling high resolution energy spectra collection during that time. The duty cycle of the control pulse is 50 percent where the gate duty cycle is 25 percent as shown in Figure 9.

Detector F was operated with the Am-241 alpha source under this pulsed configuration using frequencies from 1 to 8 mHz with the resulting spectra shown in Figure 10. The higher and lower frequencies have lower energy peak bins than the middle frequencies. The higher frequencies are most likely to exhibit charge trapping effects and the lower frequencies are more affected by polarization effects.

A pulsing frequency of 3 mHz appeared to have the highest sensitivity and sharpest peak of the frequencies tested. Smaller, thinner detectors with fewer defects are expected to have a faster biasing time and thus a faster control frequency. The role of the power supply characteristics on the biasing time and pulsing rate is unknown at this time.



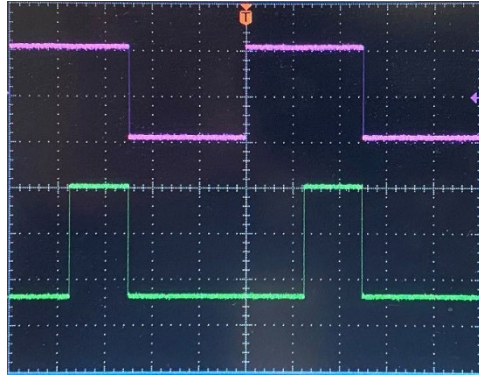


Figure 8.—Spectroscopy schematic with pulsed bias control and gated MCA data collection.

Figure 9.—Oscilloscope traces of a control pulse (top purple) and gate (bottom green).

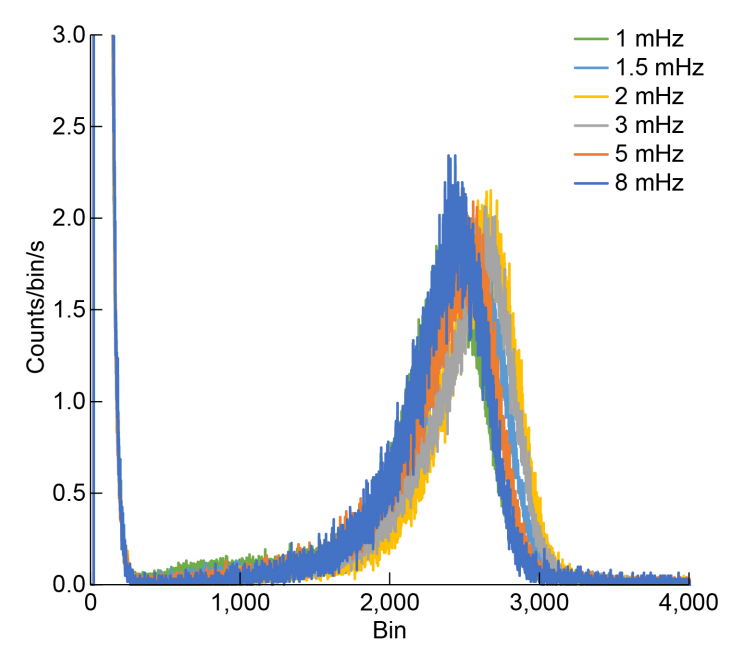


Figure 10.—Detector F spectra with Am-241 alpha source recorded using –100 V pulsed bias at various frequencies.

Testing various bias on detector F with the Am-241 alpha source at 3 mHz reveals an improvement in sensitivity and resolution than DC mode shown in Figure 11. The background, peak bin, signal to noise of the spectra, full width half maximum (FWHM) with corresponding dE/E for each bias voltage is given in Table III and plotted in Figure 12. Very little improvement in dE/E resolution is gained with voltage biasing, suggesting the source energy distribution at the detector is larger than the 0.0227 dE/E predicted by a Monte-Carlo N-Particle (MCNP, version 6.2.0) model for the energy distribution of alpha particles travelling in air from the source to the detector. The bias of –400 V had a slightly improved resolution and was selected as an optimum bias voltage for the next set of runs.

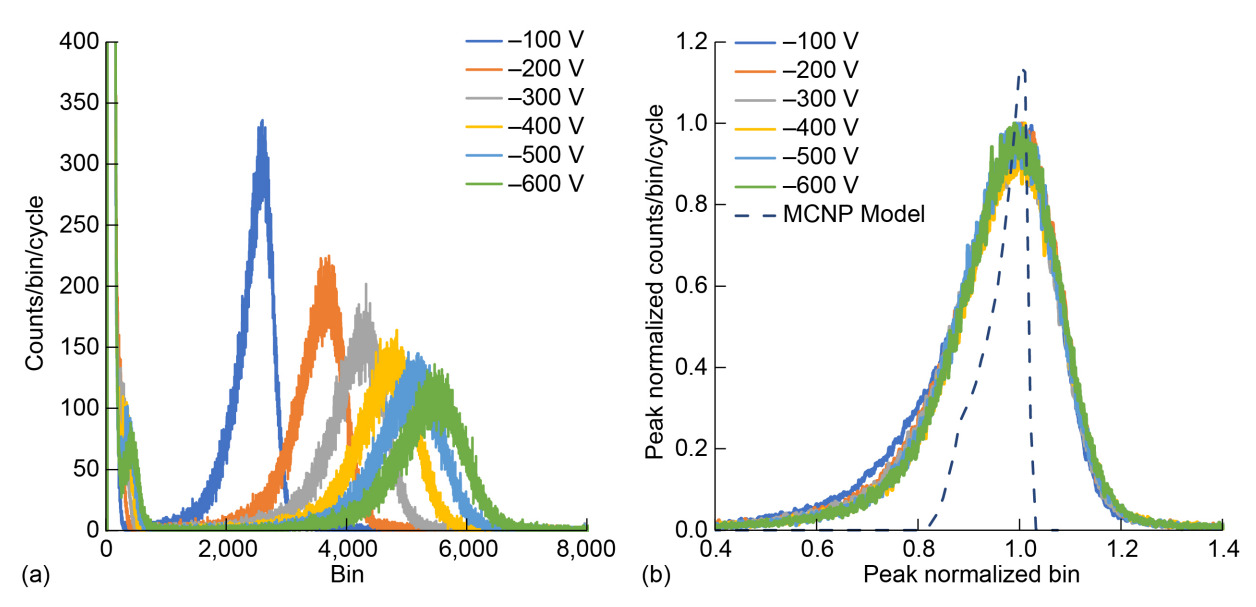


Figure 11.—Comparison of sensitivities of detector F with various 3 mHz pulsed bias voltages. (a) Collected data. (b) Data normalized to peak bin and peak counts also showing predicted spectrum generated by an MCNP model.

TABLE III.—DETECTOR F CHARACTERISTICS AT VARIOUS 3 mHz PULSED BIAS VOLTAGES

Bias (V)	Background bin (noise floor) (±1%)	Am-241 peak bin (±1%)	Signal-to-noise ratio (±2%)	FWHM bins (±2%)	dE/E (±0.02)
-100	172	2590	0.0664	556	0.0912
-200	172	3670	0.0467	816	0.0944
-300	177	4325	0.0409	932	0.0915
-400	188	4787	0.0393	1026	0.0910
-500	184	5196	0.0354	1148	0.0938
-600	186	5510	0.0338	1194	0.0920

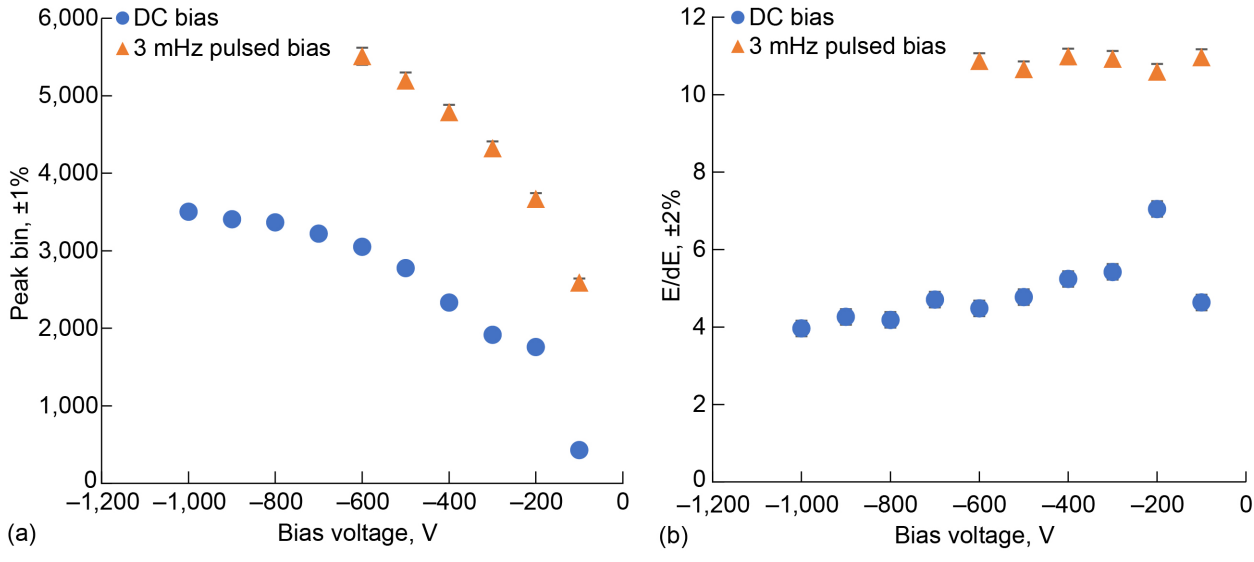


Figure 12.—Performance of detector F exposed to Am-241 alpha source at different bias in both DC and 3 mHz pulsed operation showing improvement in (a) sensitivity (peak bin) and (b) resolution (E/dE).

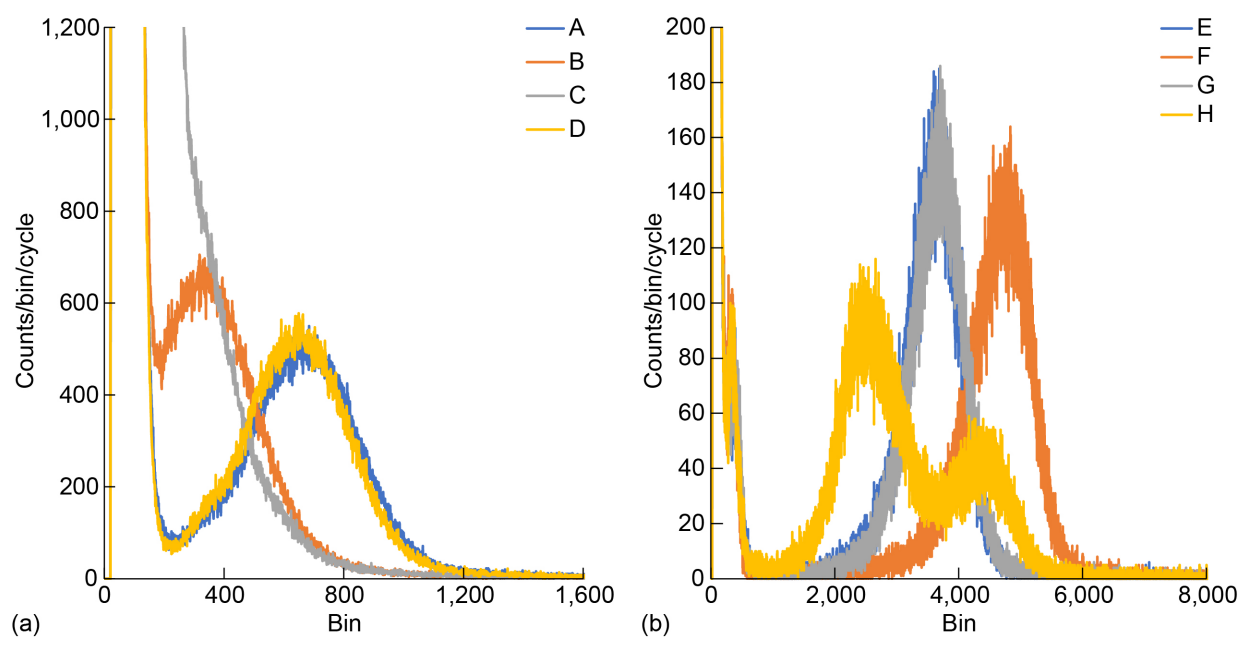


Figure 13.—Alpha spectra collected with each detector operating at –400 V, 3 mHz pulsed bias with a 166.67 s integration time. (a) Si-face detectors A-D. (b) C-face detectors E-H.

Spectra were taken using all detectors, both the Si-face set of detectors (A-D) and the C-face set of detectors (E-H). Figure 13 shows the spectra taken using -400 V, 3 mHz pulsed bias with a 166.67 s integration time. The Si-face detectors (A-D) had the signal peak appearing at bin locations that were less than 14 percent of the C-face detectors (E-H). Detector H had an unusual double peak feature as if it was behaving as two somewhat different detectors.

Metallization Analysis

To understand the difference between the front side Si-face or C-face detectors, a surface study of the metallization on both sides of the detectors was performed using Auger electron spectroscopy (AES). The resulting depth profiles are shown in Figure 14 and Figure 15.

There is no substantial difference in the front side anode metallization either sample. More silicon is visible on the Si-face than the C-face, with slightly more Pt diffusion on the Si-face, and the titanium layer is visible in both though broader in the C-face.

The back side interface is very broad for both detectors. The back side C-face shows much more diffusion of the gold than the back side Si-face, and the nickel layer is not detectable in either detector.

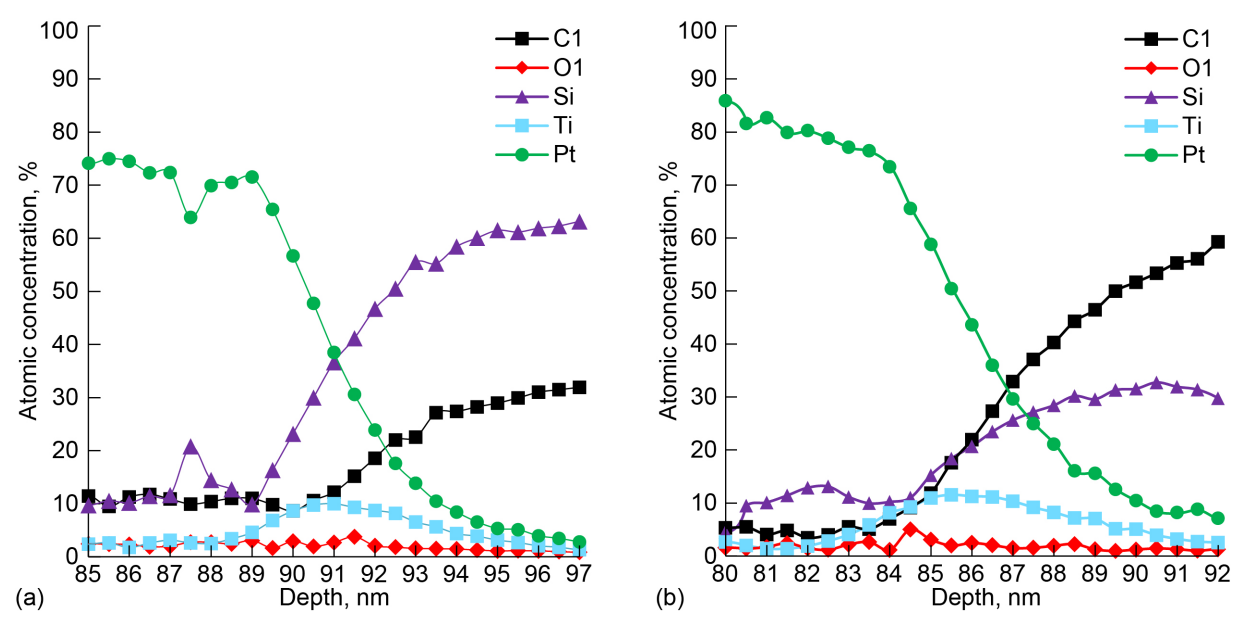


Figure 14.—AES depth profile focused on ±7 nm of metallization interface. (a) Front side Si-face detector anode metallization.

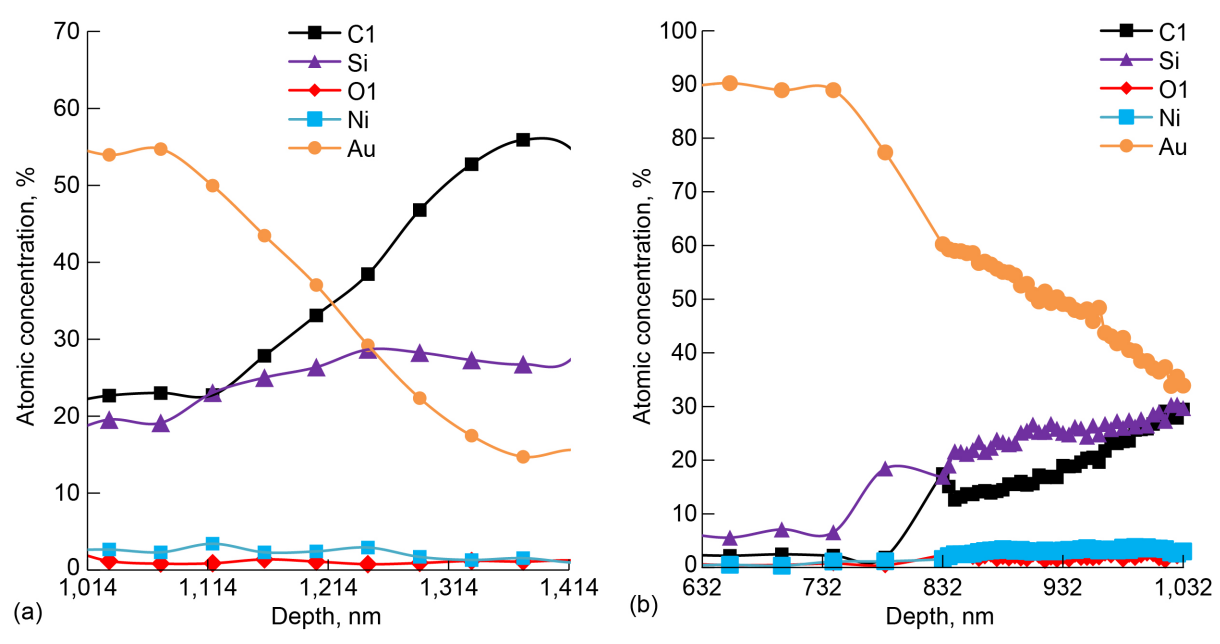


Figure 15.—AES depth profile focused on ±200 nm of metallization interface. (a) Back side C-face detector anode metallization.

Conclusions

Eight large area 2 cm² LET detectors based on 350 µm thick HPSI SiC were designed, fabricated, and characterized. These LET detectors are intended to provide a critical element to acquiring reliable information for space weather monitoring. Four detectors were fabricated using the Si-facing side of the wafer for the front side anode as well as four detectors using the C-facing side for the front side anode. A titanium-platinum anode metallization and a titanium-nickel-gold back side cathode metallization was used. The cathode metallization was annealed to 1000 °C and the anode metallization was annealed to 300 °C during fabrication.

The leakage current under -100 V negative bias was seen to range between -0.1 to -0.8 nA (± 0.1 nA), typically -0.26 nA (± 0.2 nA) regardless of type. The capacitance measurements average 58.8 ± 0.1 pF for the front side Si-face and 55.0 ± 0.1 pF for the front side C-face compared to the expected 48.9 pF for both. The higher capacitances suggest an effective thickness of the active region of the detector to be 291 µm for the front side Si-face detectors and 311 µm for the front side C-face detectors.

Response to Am-241 and Pu-239 alpha particle sources in air was documented with a multichannel analyzer recording the relative peak heights. The detectors with the front side Si-face anode were found to have 14 percent the sensitivity of those using the front side C-face anode.

Polarization effects were observed with a -0.1 percent per minute drift after biasing for over 2 h, limiting dE/E resolution to 0.14 at -200 V bias. Pulsing the bias at 3 mHz found an improvement of resolution to a dE/E of 0.0923 ± 0.0014 regardless of biasing, suggesting that resolution is primarily limited by the energy dispersion of the alpha particles in air, and is a significant improvement over performance recorded by previous iterations.

Finally, depth analysis of the anode and cathode metallization layers were examined. Though there was no significant difference between the front side C-face and Si-face anodes, the back side C-face cathodes shows much more diffusion of the gold than the back side Si-face cathodes, and the nickel layer is not detectable in either detector.

In summary, improvements in large-area HPSI SiC LET detectors for space science applications have been demonstrated to include lower leakage current and better particle energy resolution. Polarization effects have been demonstrated to be mitigated through pulsed biasing of the detectors. The presence of silicon as part of the electrode metallization has been shown to affect the performance as well.

References

- 1. Schwadron, N.A., et al. (2012) "Lunar Radiation Environment and Space Weathering from the Cosmic Ray Telescope for the Effects of Radiation (CRaTER)," J. Geophys. Res.-Planets 117, E00H13.
- 2. Marsh, N.D. and H. Svensmark (2000) "Low Cloud Properties Influenced by Cosmic Rays." Phys. Rev. Lett. 85 (23) 5004-5007.
- 3. Tribble, A.C. (2003) The Space Environment: Implications for Spacecraft Design (Princeton University Press).
- 4. Mulligan, T., J.B. Blake, D. Shaul, J.J. Quenby, R.A. Leske, R.A. Mewaldt, and M. Galametz (2009) "Short-period variability in the galactic cosmic ray intensity: High statistical resolution observations and interpretation around the time of a Forbush decrease in August 2006," J. Geyophys. Res. 114, A07105.
- 5. Vourlidas, A., et al. (2021) "Space Weather Science and Observation Gap Analysis for the National Aeronautics and Space Administration (NASA)," Johns Hopkins Applied Physics Laboratory. https://science.nasa.gov/wp-content/uploads/2024/09/gapanalysisreport-full-final-tagged.pdf

- 6. Wrbanek, J.D. and Wrbanek, S.Y. (2020) "Space Radiation and Impact on Instrumentation Technologies," NASA/TM—2020-220002.
- 7. Nava, F., G. Bertuccio, A. Cavallini, and E. Vittone (2008), "Silicon carbide and its use as a radiation detector material." Meas. Sci. Technol., vol. 19, 102001.
- 8. Ruddy, F.H., A.R. Dulloo, J.G. Seidel, S. Seshadri, and L.B. Rowland (1998) "Development of a Silicon Carbide Radiation Detector," IEEE Trans. Nucl. Sci. 45 (3) 536-541.
- 9. Wrbanek, J.D., G.C. Fralick, S.Y. Wrbanek, and L.Y. Chen (2007) "Micro-fabricated solid-state radiation detectors for active personal dosimetry." NASA/TM—2007-214674.
- 10. G.R. Thomas and D.M. Willis, "Analytical derivation of the geometric factor of a particle detector having circular or rectangular geometry," J. Phys. E: Sci. Inst. 5 (3) 260-263 (1972).
- 11. Wrbanek, J.D. and Wrbanek, S.Y. (2016) "Multidirectional Cosmic Ray Ion Detector for Deep Space CubeSats," Proceedings of the AIAA/USUS Conference on Small Satellites, Advanced Technologies I, SSC16-IV-2.
- 12. Knoll, G.F. (2000) Radiation Detection and Measurement, Third Edition (John Wiley & Sons, Inc.)
- 13. Lutz, G. (1999) Semiconductor Radiation Detectors (Springer).
- 14. LibreTexts "B1: Workfunction Values (Reference Table)" https://chem.libretexts.org/Ancillary_Materials/Reference/Reference_Tables/Bulk_Properties/B1%3 A Workfunction Values (Reference Table) Accessed February 12, 2024.
- 15. Mekaret, F. et al. (2024) "A comparative study of Schottky barrier heights and charge transport mechanisms in 3C, 4H, and 6H silicon carbide" AIP Advances 14, 115302. https://doi.org/10.1063/5.0240123
- 16. Crofton, J., P.G. McMullin, J.R. Williams, and M.J. Bozack (1995) "High-temperature ohmic contact to n-type 6H-SiC using nickel," J. Appl. Phys. 77, 1317. https://doi.org/10.1063/1.358936.
- 17. Liu, L., Ao Liu, Son Bai, Ling Lv, Peng Jin, and Xiaoping Ouyang (2017) "Radiation Resistance of Silicon Carbide Schottky Diode Detectors in D-T Fusion Neutron Detection," Sci. Rep. 7, 13376. https://doi.org/10.1038/s41598-017-13715-3
- 18. Ruddy, F.H., J.G. Seidel, R.W. Flammang, R. Singh, and J. Schroeder (2008) "Development of Radiation Detectors Based on Semi-Insulating Silicon Carbide," IEEE Nucl. Sci. Symp. Conf. Rec. 449-455.
- 19. Rafí, J.M., et al., (2020) "Electron, Neutron, and Proton Irradiation Effects on SiC Radiation Detectors," IEEE Trans. Nucl. Sci. 67 (12) 2481-2489. doi: 10.1109/TNS.2020.3029730
- 20. Cunningham, W., A. Gouldwella, G. Lamb, et al. (2002) "Performance of bulk SiC radiation detectors," Nucl. Inst. Meth. Phys. Res. A 487, 33-39.
- 21. Radulović, V., Y. Yamazaki, Ž. Pastuović, et al. (2020) "Silicon carbide neutron detector testing at the JSI TRIGA reactor for enhanced border and port security," Nucl. Inst. Meth. Phys. Res. A 972, 164122. https://doi.org/10.1016/j.nima.2020.164122
- 22. Patrick, Lyle and Choyke, W.J. (1970) "Static Dielectric Constant of SiC," Phys. Rev. B 2(6) 2255-2256. https://doi.org/10.1103/PhysRevB.2.2255
- 23. P.V. Raja, J. Akhtar, C.V.S. Rao, S. Vala, M. Abhangi, and N.V.L.N. Murty (2017) "Spectroscopic performance studies of 4H-SiC detectors for fusion alpha-particle diagnostics," Nuclear Inst. and Methods in Physics Research, A 869 (2017) 118–127 http://dx.doi.org/10.1016/j.nima.2017.07.017
- 24. Ibragimov et al. (2016) J. Phys.: Conf. Ser. 675 042013, https://doi.org/10.1088/1742-6596/675/4/042013
- 25. Holmes, et al. (2019) Diam. Relat. Mater. 94 162-165, https://doi.org/10.1016/j.diamond.2019.01.025